The Astronomical Journal, 150:196 (9pp), 2015 December doi:10.1088/0004-6256/150/6/196

AGN ACTIVITY AND IGM HEATING IN THE FOSSIL CLUSTER RX J1416.4+2315

H. Miraghaei[1,2], H. G. Khosroshahi[1], C. Sengupta[3], S. Raychaudhury[4,5], N. N. Jetha[6], and S. Abbassi[1,7]
[1] School of Astronomy, Institute for Research in Fundamental Sciences, P.O. Box 19395-5531, Tehran, Iran; halime@ipm.ir
[2] Department of Physics, Sharif University of Technology P.O. Box 11365-9161, Tehran, Iran
[3] Korea Astronomy and Space Science Institute, 776, Daedeokdae-ro, Yuseong-gu, Daejeon 305-348, Korea
[4] Department of Physics, Presidency University, 86/1 College Street, 700 073 Kolkata, India
[5] School of Physics and Astronomy, University of Birmingham, Edgbaston, Birmingham B15 2TT, UK
[6] Center for Space Plasma and Aeronomic Research (CSPAR), University of Alabama in Huntsville, Huntsville, AL 35805, USA
[7] Department of Physics, School of Sciences, Ferdowsi University of Mashhad, Mashhad 91775-1436, Iran
Received 2014 February 19; accepted 2015 September 27; published 2015 December 11

ABSTRACT

We study active galactic nucleus (AGN) activity in the fossil galaxy cluster RX J1416.4+2315. Radio observations were carried out using the Giant Metrewave Radio Telescope at two frequencies, 1420 and 610 MHz. A weak radio lobe that extends from the central nucleus is detected in the 610 MHz map. Assuming the radio lobe originated from the central AGN, we show that the energy injection into the intergalactic medium is only sufficient to heat up the central 50 kpc within the cluster core, while the cooling radius is larger (∼130 kpc). In the hardness ratio map, three low energy cavities have been identified. No radio emission is detected for these regions. We evaluated the power required to inflate the cavities and showed that the total energy budget is sufficient to offset the radiative cooling. We showed that the initial conditions would change the results remarkably. Furthermore, the efficiency of the Bondi accretion in powering the AGN has been estimated.

Key words: galaxies: active – galaxies: clusters: individual (RX J1416.4+2315) – intergalactic medium – radio continuum: galaxies

1. INTRODUCTION

The intergalactic medium (IGM) heating is one of the challenging issues in observational cosmology. Many galaxy groups and clusters have been found to contain hot intergalactic gas, most of which have cooling timescales longer than the Hubble time. The cooling time in the core of many galaxy groups and clusters is, however, much shorter than the Hubble time. While it was argued that this gas should cool dramatically to very low temperatures (Fabian et al. 1984; Sarazin 1986; Fabian et al. 1991), challenges were posed by X-ray observations of *XMM-Newton* and *Chandra* when they found no evidence of a catastrophic cooling, suggesting that one or more processes are stopping the gas from cooling below a certain (∼0.5 keV) temperature (see Peterson & Fabian 2006 and references therein).

Active galactic nuclei (AGNs) are seen as a primary source of heating, mainly because they appear to be present in most cool core galaxy groups and clusters (Mittal et al. 2009). AGNs interact with the intergalactic gas by sending radio jets, bubbles, shocks, and sound waves powered by supermassive black holes (SMBHs) and heat the IGM via different mechanisms (Gaspari et al. 2011). Among all the heating sources introduced up to now, bubble structures are the main supporting evidence for AGN heating (Bîrzan et al. 2004, 2008; Dunn & Fabian 2004; Dunn et al. 2005, 2010; Rafferty et al. 2006; Nulsen et al. 2007; Sanders et al. 2009; Cavagnolo et al. 2010; O'Sullivan et al. 2011). Radio bubbles release a huge amount of energy into the IGM in the form of mechanical work. The energy required to inflate a bubble is roughly 10^{55} erg in low mass systems and up to 10^{61} erg in rich clusters. Recent studies of X-ray cavities show that mechanical heating provides sufficient energy to quench the cooling rate in most of the cooling flow groups and clusters up to $z \sim 0.8$ (Hlavacek-Larrondo et al. 2012, 2015).

The accretion flow onto the black hole prompts the relativistic jets and lobes into the IGM. There are two modes of accretion into the SMBH that are assumed to contribute to the AGN power, the accretion of cold optically thick gas occurring at a high accretion rate and hot optically thin accretion of gas at a low accretion rate (Yuan & Narayan 2014). The latter is believed to operate radio mode feedback in galaxy clusters and groups. Additionally, galaxy simulations show that mergers or instability caused by galaxy interactions excite gas infall and fuel black hole growth (Springel et al. 2005a, 2005b). Observational restrictions do not allow us to determine which type of accretion mode is induced by the galaxy mergers since the accretion mode is mainly determined by the boundary condition of the gas at the Bondi radius (Yuan & Narayan 2014). When the black hole reaches a critical mass, the feedback blows out material from the central region and regulates the black hole growth. A study by Ellison et al. (2011) shows a clear increase in the AGN fraction in close pairs of galaxies. Therefore, mergers of galaxies trigger AGN activity and consequently heat the IGM. Moreover, the energy released by a galactic merger (∼10^{64} erg) is enough to disturb cool cores (Markevitch et al. 1999; Gómez et al. 2002; Markevitch & Vikhlinin 2007; McNamara & Nulsen 2007). So, the heating role of galaxy mergers is important to account for the heating and cooling balance inside the group.

Galaxy clusters and groups are evolving systems and a galactic merger is a built-in process in these systems. However, there is a class of galaxy groups in which major mergers are thought to have taken place on timescales much larger than the return period of the AGN activities. Such galaxy groups are known as fossil groups, which are dominated optically by a single luminous elliptical galaxy at the center of an extended luminous X-ray emission similar to those seen in bright X-ray groups. The X-ray emission in fossils is usually regular and symmetric, indicating the absence of recent group scale

merging. Apart from the observational indications pointing to the early formation of fossil galaxy groups (Khosroshahi et al. 2006a, 2006b, 2007), cosmological simulations also show that fossil group halos are formed relatively earlier (Dariush et al. 2007, 2010) than the general population of the groups and clusters with a similar halo mass.

Two main advantages of studying AGN feedback in fossil groups are the following. (a) The central giant elliptical galaxy has not experienced a recent galactic merger and, given the absence of any bright nearby galaxies, is not subject to any major instability due to interactions with massive surrounding galaxies. (b) The cluster itself has not experienced any large scale merger which can disturb the formation of the cool core. Fossils are thus thought to be relatively simple laboratories to study AGN feedback. This study is focused on the radio properties of one of the most massive fossil groups known in the local Universe, RX J1416.4+2315 (hereafter J1416) at $z \approx 0.137$. This group contains one of the most massive giant ellipticals known and has been studied as part of a volume limited sample of spatially extended X-ray sources compiled during the Wide Angle *ROSAT* Pointed Survey project (Scharf et al. 1997; Jones et al. 1998; Perlman et al. 2002). It is the most X-ray luminous source in the sample of five fossil groups studied by Jones et al. (2003), with a *ROSAT* estimated X-ray bolometric luminosity of 1.1×10^{44} erg s^{-1}. In a deep optical image it would be classified as a galaxy group or poor cluster centered on an extremely dominant, luminous giant elliptical galaxy (Khosroshahi et al. 2006a).

In Section 2 we describe the radio observation and morphology. X-ray morphology is presented in Section 3. Estimation of the heat budget is described in Section 4. The synchrotron aging and black hole accretion are presented in Sections 5 and 6, respectively. A summary and discussion are given in Section 7. Throughout this paper we assume a ΛCDM cosmology with $\Omega_m = 0.27$, $\Omega_\Lambda = 0.73$, and $H_0 = 100h$ km s^{-1} Mpc^{-1} where $h = 0.71$.

2. RADIO OBSERVATION AND MORPHOLOGY

The cluster was imaged in two frequencies, 1420 and 610 MHz, with the Giant Metrewave Radio Telescope (GMRT) to study a possible correlation of the spatial features of the IGM in radio and X-ray. The system temperature, gain (K Jy^{-1}), and FWHM of the primary beam of the instrument in 1420 MHz are ∼76 K, 0.22, and 24′, respectively, and in 610 MHz are 92 K, 0.32, and 54′, respectively. The source was observed on 2005 July 4 and 5 for 10 hr in 1420 MHz and on July 11 and 12 for 10 hr in 610 MHz.

The data were reduced using the Astronomical Image Processing System (AIPS). Bad data, e.g., dead antennas, antennas with significantly lower gain, and bad time, were removed and the data was calibrated for flux and phase using 3C286 as a primary calibrator in both frequencies and 1407 +284 and 3C287 as secondary calibrators in 1420 MHz and 610 MHz, respectively. Imaging was performed using the AIPS task "IMAGR." Polyhedron imaging was performed to take care of the well known problem of wide field imaging in low frequencies. Map rms ∼130 μJ and ∼180 μJ were reached in 1420 MHz and in 610 MHz, respectively.

In 1420 MHz, a source was detected at the position of R.A.: $14^h16^m27\overset{s}{.}47$ and decl.: $+23°15'22\overset{''}{.}40$. The peak flux of this source is 2.60 ± 0.13 mJy beam^{-1}. This is in agreement with the source from the FIRST catalog detected at the position of R.A.: $14^h16^m27\overset{s}{.}39$ and decl.: $+23°15'23\overset{''}{.}00$, with a peak flux of 2.36 ± 0.145 mJy beam^{-1} and with the source from the NVSS catalog at the position of R.A.: $14^h16^m29^s$ and decl.: $+23°15'28''$,with a peak flux of 3.1 ± 0.5 mJy beam^{-1}. High and low resolution images of this source at 1420 MHz have been presented in Figures 1 and 2. Details of the maps are given in Table 1.

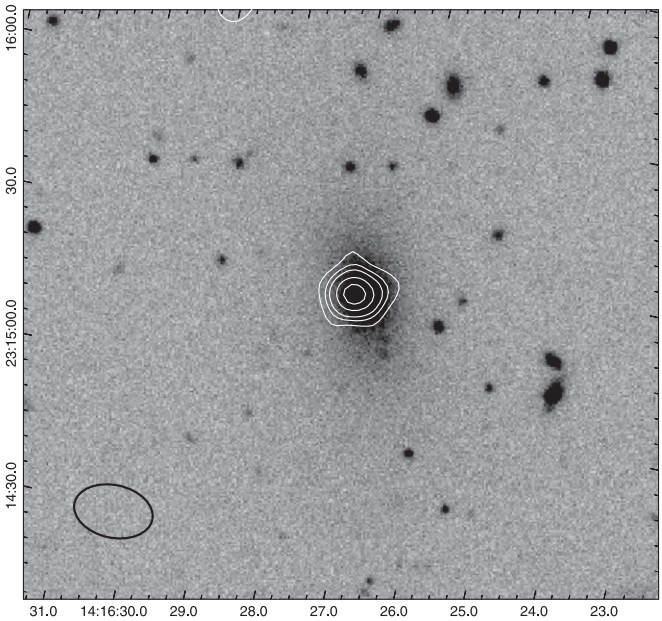

Figure 1. 1.4 GHz high resolution radio map of the source overlaid on the SDSS optical image of the central galaxy, RX J1416.4+2315. Contour levels of 0.45, 0.75, 1.05, 1.65, and 2.25 mJy are shown. The synthesized beam is shown on the bottom-left of the image.

In 610 MHz, two sources were detected in the high resolution image: a peak at the position of R.A.: 14 16 27.35, decl.: +23 15 22.00 (hereafter the central source) and a second peak at R.A.: 14 16 27.64, decl.: +23 15 18.00 (hereafter the radio counterpart). The peak flux for the central source is 4.29 ± 0.13 mJy beam^{-1} and for the radio counterpart is 2.00 ± 0.2 mJy beam^{-1}. High and low resolution images of this source at 610 MHz are shown in Figures 3 and 4. The nature of the radio counterpart is unclear. There is no point source in the X-ray map associated with this structure. Given the alignment (along the minor axis of the central giant elliptical), it can be a remnant from the previous outburst. No counterparts are apparent either on the SDSS image (magnitude limit $m_r < 17.7$) or on the 2MASS image (point-source limiting magnitude Ks < 14.3). Thus, in this study, we assume that this source is a radio lobe inflated by the central AGN. Given the 1420 MHz flux, the spectral index ($S \propto \nu^{-\alpha}$) calculated for the central source is 0.83. If the same spectral index is assumed for the radio lobe, the source is expected to have a 3σ detection in the 1420 MHz image, given that the map rms is ∼130μ Jansky.

The presence of diffused extended emission was checked by subtracting the high resolution integrated flux density of the source from the low resolution image. At 1420 MHz, no residual flux was found, indicating that the emission is dominated by a central compact source. Subtracting the FIRST flux density from the NVSS flux density also confirms it

Table 1
Details of the Radio Measurements of RX J1416.4+2315

Frequency (MHz)	Position J2000	Peak Flux (mJy)	Integrated Flux (mJy)	Map rms (mJy)	Resolution (arcsec)
610	$14^h16^m27\overset{s}{.}357$ $+23°15'22\overset{''}{.}00$	4.29 ± 0.13	7.10 ± 0.33	0.18	8.03 × 5.36
610	$14^h16^m\ 27\overset{s}{.}647$ $+23°15'18\overset{''}{.}00$	2.00 ± 0.20	2.08 ± 0.20	0.18	8.03 × 5.36
610	$14^h16^m27\overset{s}{.}502$ $+23°15'24\overset{''}{.}00$	7.60 ± 0.65	12.41 ± 1.60	0.98	40.39 × 34.28
1420	$14^h16^m27\overset{s}{.}473$ $+23°15'22\overset{''}{.}40$	2.60 ± 0.13	3.55 ± 0.27	0.13	8.30 × 6.96
1420	$14^h16^m27\overset{s}{.}502$ $+23°15'22\overset{''}{.}00$	3.40 ± 0.43	3.48 ± 0.76	0.36	32.98 × 29.78

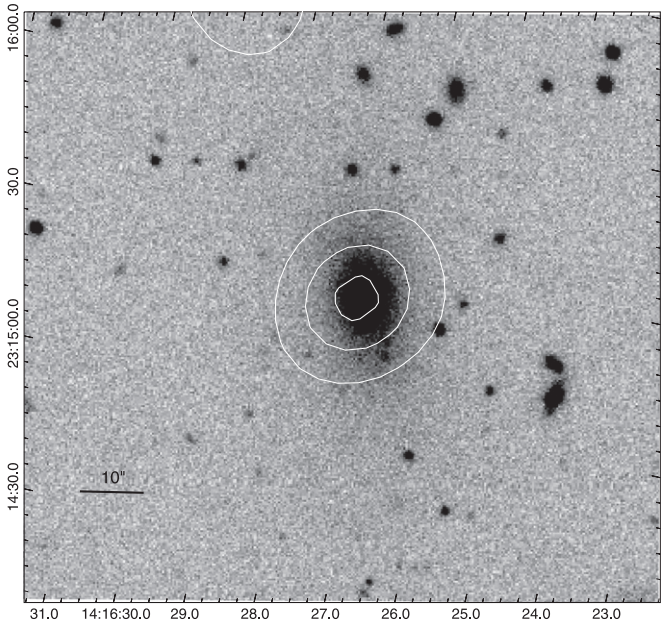

Figure 2. 1.4 GHz low resolution radio map of the source overlaid on the SDSS optical image of the central galaxy, RX J1416.4+2315. Contour levels of 0.0015, 0.0025, and 0.0032 Jy are shown.

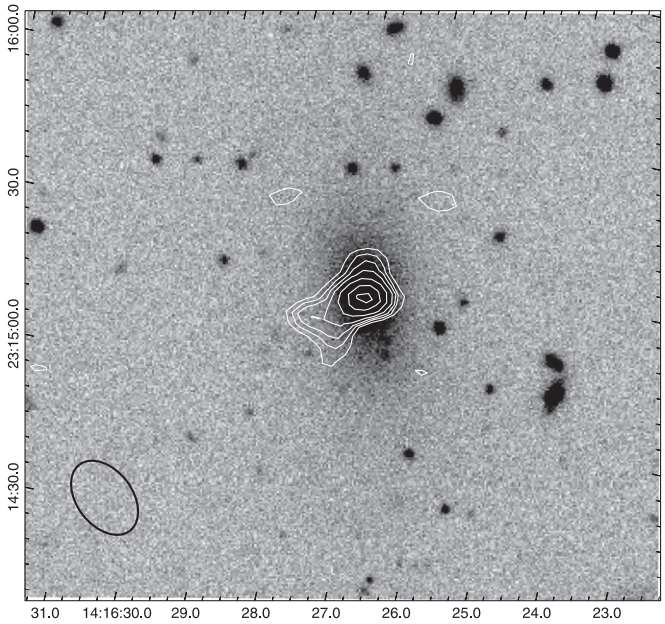

Figure 3. 610 MHz high resolution radio map of the source overlaid on the SDSS optical image of the central galaxy, RX J1416.4+2315. Contour levels of 0.66, 0.88, 1.42, 2.0, 3.0, and 4.0 mJy are shown. The synthesized beam is shown on the bottom-left of the image.

(Table 2). At 610 MHz, there is a ∼3 mJy residual that indicates the presence of diffused emission.

3. X-RAY MORPHOLOGY

An X-ray data analysis of J1416 has been reported in Khosroshahi et al. (2006a). We used the results of *Chandra* and *XMM-Newton* observations in this study. Throughout the paper, X-ray luminosities have been estimated by integrating over the surface brightness profile. A two-dimensional β-model fit to the *Chandra* data has been used for this aim. In order to obtain the electron density (n_e), the deprojected luminosity of 3D shells with a fixed radius was combined with the model emissivity ϵ at the shell temperature (and in the same energy band, 0.3–2.5 keV) and the shell volume V, via

$$L = n_e n_H V \epsilon. \quad (1)$$

For the hydrogen number density we assumed $n_e = 1.17 n_H$. The deprojected temperature profile is reported in Khosroshahi et al. (2006a). We estimated the pressure using the equation $p = \frac{kT\rho}{\mu m_p}$ for the perfect gas, with k being the Boltzmann constant, μ the mean molecular weight, and m_p the atomic mass constant. For the gas density, we assumed $\rho = 1.17 n_e m_p$ according to Reiprich (2001).

X-ray soft (0.5−2 keV) diffuse emission from *XMM-Newton* with 610 MHz radio contours is shown in Figure 5. The diffuse emission image was produced by adaptively smoothing an exposure-corrected image of the emission detected by the three *XMM-Newton* EPIC cameras. There is a SW tail in the same direction as the radio lobe. Compared to the X-ray emission at the same radius, the tail is ∼40% brighter with a 6σ significance level.

A soft diffuse *Chandra* image (0.3–2.0 keV) is shown in Figure 6. The point sources are removed and the emission has been smoothed with a two-dimensional Gaussian function, σ = 5 pixels (∼5″ kernel radius). The image shows a depression in the surface brightness map in the direction of the radio lobe. To assess the significance of this cavity, we

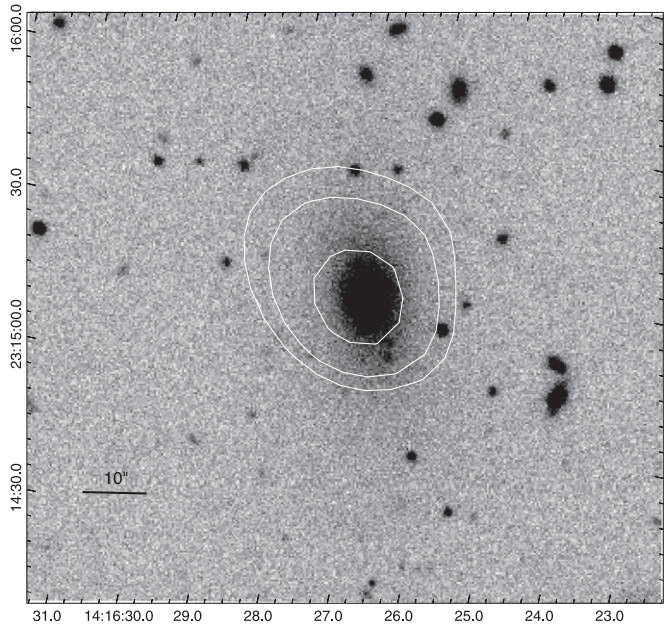

Figure 4. 610 MHz low resolution radio map of the source overlaid on the SDSS optical image of the central galaxy, RX J1416.4+2315. Contour levels of 0.004, 0.005, 0.007, and 0.0079 Jy are shown.

Table 2
1420 MHz Radio Measurements of RX J1416.4+2315

Catalog	Peak Flux (mJy)	Integrated Flux (mJy)	Map rms (mJy)
GMRT	2.60	3.55	0.13
FIRST	2.36	3.39	0.145
NVSS	3.1	3.6	0.5

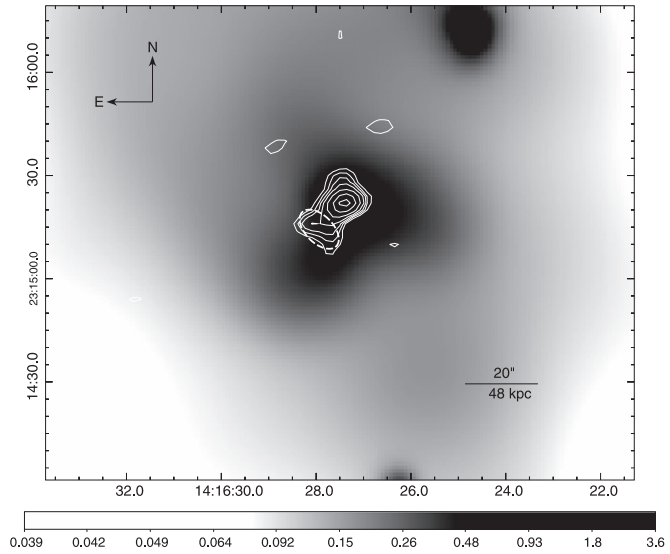

Figure 5. X-ray smooth emission (∼10″ kernel radius) from the *XMM-Newton* observations of cluster RX J1416.4+2315 with 610 MHz radio contours. The dashed ellipse demonstrates the bubble size used for the volume estimation.

averaged the counts per pixel over the cavity surface (marked as A) and the regions of the same radius from the center (marked as B). The mean value for the cavity is 0.085 ± 0.009 (counts pixel^{-1}) compared to 0.112 ± 0.022 (counts pixel^{-1}) for region B. The surface brightness depression is weaker than

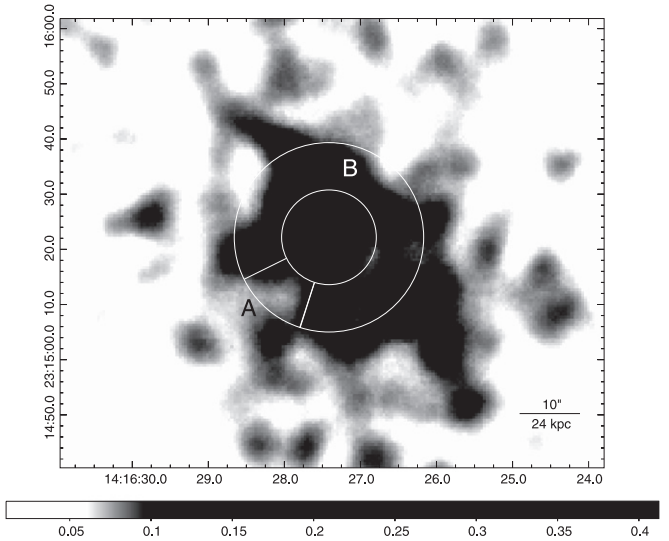

Figure 6. X-ray emission of the cluster from *Chandra* observations. There is a depression in region A where the radio contours show the existence of a radio lobe. The image has been smoothed with 5″ kernel radius.

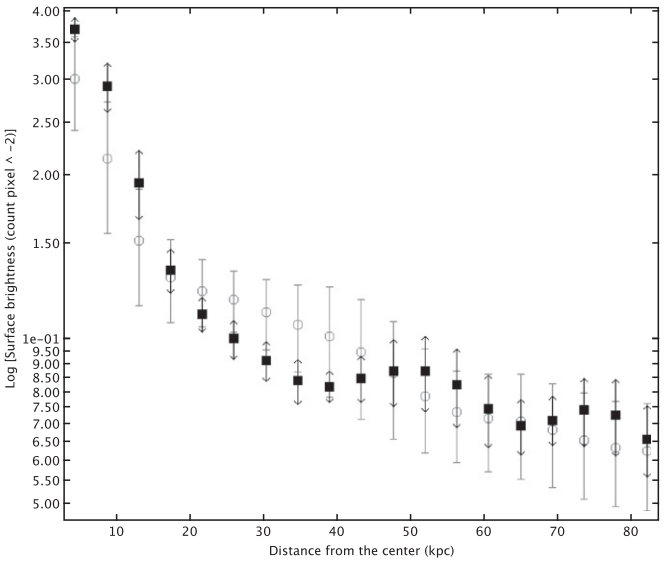

Figure 7. X-ray surface brightness profile of the cluster from *Chandra* observations (open circle) and the same trough in the direction of the radio lobe (filled square). There is a weak depression around ∼30 kpc which is uncertain according to the error bars.

the noise level in the X-ray map. Thus, the reliablity of the depresstion cannot be investigated with the current X-ray data. Figure 7 shows the surface brightness profile of the entire cluster (open circle) and through the direction of the radio lobe (filled square). The bin size has been adjusted to the resolution of the X-ray image. The *Y* axis represents the mean of the surface brightness in each bin with the standard deviation of each bin as the error bar. A small depression around ∼30 kpc is again uncertain due to the huge error bars.

The hardness ratio map is shown in Figure 8. The soft image contains photons with energies from 400 to 900 eV. The hard image consists of photons with energies ranging from 900 eV to 2 keV. Before deriving the hardness ratio map, we replaced the point sources using their surrounding counts and applied smoothing on the hard and soft band with the scale of an 8 × 8 binned image using the csmooth task in CIAO. The

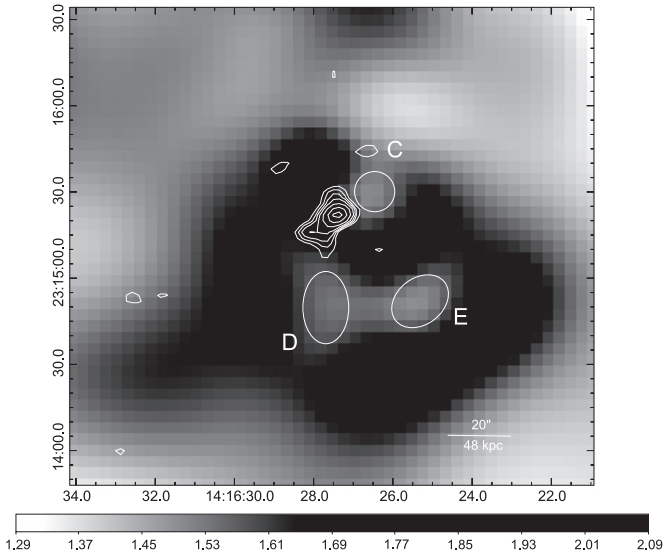

Figure 8. Hardness ratio map from the *XMM-Newton* observations. Three cavities are marked in this map (C, D, and E). 610 MHz radio contours are also shown. The image has been smoothed with 10″ kernel radius.

corresponding backgrounds were subtracted from the soft and hard images. The bubble-like low energy cavities are seen in the south (marked as D and E) and northwest (marked as C). In order to explore the reliability of these cavities, we compared the hardness ratio inside these regions with their surroundings by averaging the count per pixel in each cavity and an annulus around it (not shown in Figure 8 to prevent confusion). The level of deficiency of the cavities is presented in Table 3 and shows that surface brightness depressions are real in all cases. Figures 9–11 show hardness ratio profile of the entire cluster (open circle) and through the direction of cavities C, D, and E, showing clear depressions around ∼20 kpc, ∼50 kpc, and ∼80 kpc, respectively. The bin size and the error bars are the same as in Figure 7. The cavities are possibly due to multiple cycles of AGN outflows. However, no radio emission is detected in any of these regions.

4. AGN HEATING

X-ray observations of clusters and groups of galaxies reveal that most of the cooling flow clusters and groups have cavities defined by a depression in their X-ray surface brightness. These cavities are filled with radio bubbles consisting of relativistic particles and magnetic fields when observed at low frequencies. Such observations are consistent with the current scenario in which AGN activity at the center of clusters and groups inflates the bubbles into the IGM, fed by powerful radio jets. A large number of studies suggest that AGNs as a prominent source of heating can quench cooling rates through various processes (Fabian et al. 2006; Heinz et al. 2006; McNamara & Nulsen 2007; Blanton et al. 2010). *PdV* work by the inflated bubbles on the surrounding medium can be a lower limit in the heat supply (Begelman 2001; Churazov et al. 2002; Nusser et al. 2006). Other mechanisms will boost the heating and possibly explain the lack of cool gas in the cluster core.

From the cavity enthalpy we have

$$H = E + PV = \frac{\gamma}{\gamma - 1} PV, \tag{2}$$

Table 3
Hardness Ratio Map, Cavity Characteristics

Cavity	Cavity Hardness Ratio	Anullus Hardness Ratio	t_c (10^7 years)	P_c (10^{43} erg s^{-1})
C	1.519 ± 0.015	1.607 ± 0.060	3.9	4.3
D	1.551 ± 0.015	1.662 ± 0.073	8.6	4.3
E	1.548 ± 0.036	1.698 ± 0.053	11.1	3.6

in which we assumed the perfect gas relation for the internal energy of the cavity:

$$E = \frac{1}{\gamma - 1} PV. \tag{3}$$

Here, $\gamma = 4/3$ is the adiabatic index for the relativistic particles. In this study, we assume that the radio bubble is formed near the center of the group with an overpressure factor of p_0/p (where p_0 is the initial pressure of the bubble and p is the ambient pressure and also the bubble final pressure, assuming the bubble pressure reaches the ambient pressure in the last stage of expansion) and then moves to the observed position with the pressure and the volume P and V. The enthalpy change of the bubble during this process is given by

$$\Delta H = \frac{\gamma}{\gamma - 1} PV \left[\left(\frac{p_0}{p} \right)^{1-1/\gamma} - 1 \right]. \tag{4}$$

This is based on the adiabatic assumption $PV^\gamma = \text{const}$ and is consistent with rapid expansion of the bubble.

Observations of J1416 in 610 MHz detected a radio source at the southeast of the cluster center, but no such emission was detected at this position in 1420 MHz. The distance between the position of the peak flux density of the central source and the radio lobe is approximately 28 kpc. The absence of detection of any radio lobe in 1420 MHz shows that this source has a steep spectrum up to $\alpha \sim 2$ compared to the central radio emission ($\alpha = 0.83$). Steepening of about 0.5 is expected at high frequency as a result of synchrotron aging (Feretti & Giovannini 2008). Further discussion is presented in Section 5.

The spatial resolution of *XMM-Newton* is barely sufficient for detecting any X-ray cavities at this distance from the central X-ray point source. The *Chandra* X-ray telescope, which has much better spatial resolution, shows a weak deficiency in the X-ray surface brightness associated with the radio lobe (Figures 6 and 7). The binning and smoothing is minimal to enable us to see small scale surface brightness variations in this map. As we discussed in Section 3, the depression is not reliable due to the huge error bars. Thus, we used radio data to evaluate bubble dimensions.

Here, we estimate the energy required to inflate the radio lobe (bubble heating) using Equation (4) and discuss the heating and cooling balance at the center of this cluster. The bubble has an approximately elliptical shape with a semimajor axis of 16 kpc and semiminor axis of 9 kpc (shown in Figure 5). The extent of the source is calculated by fitting a Gaussian function to the image using the AIPS task JMFIT. We assume a mean radius of $r = \sqrt{ab}$ for the bubble where a and b are the semiminor and semimajor axes of the ellipse, respectively. The ambient pressure is $p = 1.6{-}1.7 \times 10^{-11}$ dyn cm^{-2} at a 28 kpc radius from the center (the current position of the radio bubble).

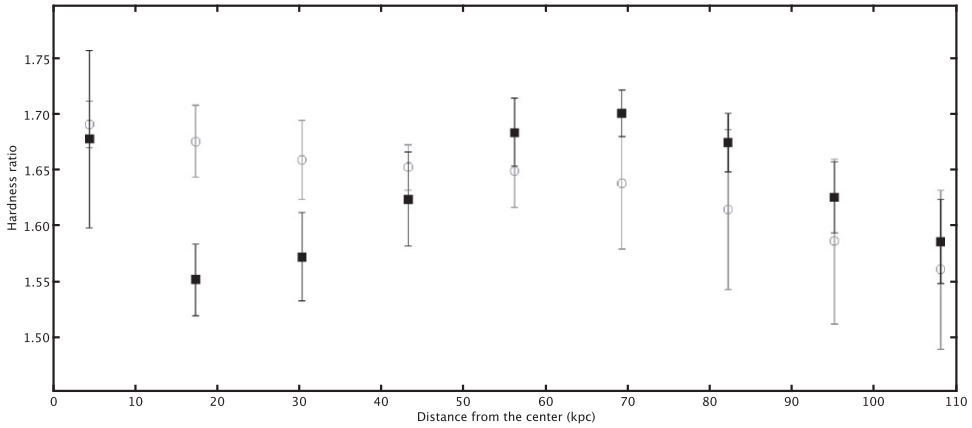

Figure 9. Hardness ratio profile of the cluster (open circles) and the same trough in the direction of cavity C (filled square). There is a real depression around ∼20 kpc, consistent with the cavity position.

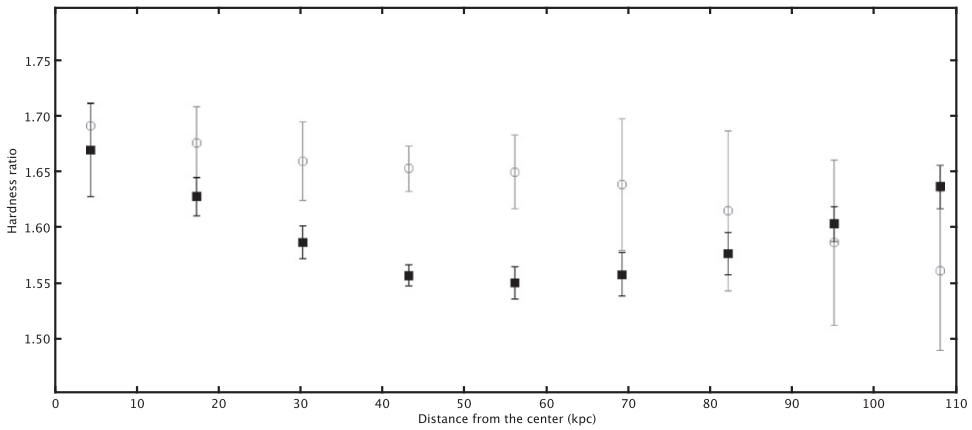

Figure 10. Hardness ratio profile of the cluster (open circles) and the same trough in the direction of cavity D (filled square). There is a real depression around ∼50 kpc, consistent with the cavity position.

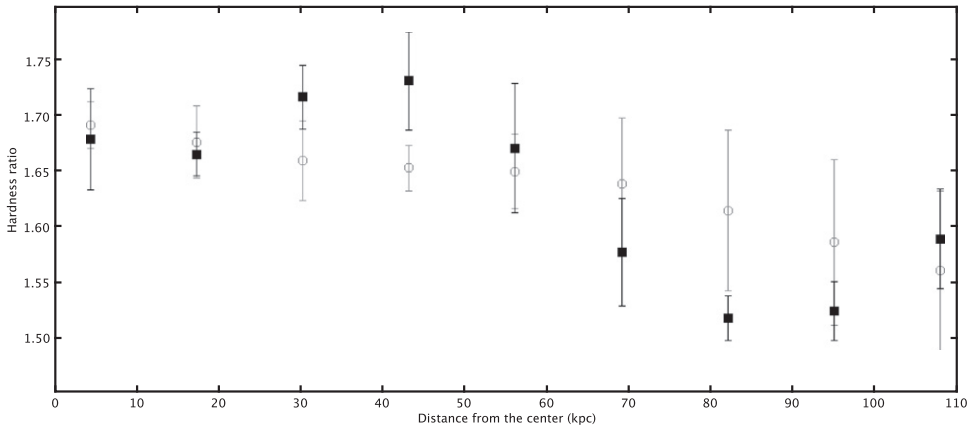

Figure 11. Hardness ratio profile of the cluster (open circles) and the same trough in the direction of cavity E (filled square). There is a real depression around ∼80 kpc, consistent with the cavity position.

The enthalpy change is $\Delta H = 2.6 \times 10^{57}$ erg assuming an overpressure factor of 2 and $\Delta H = 10.6 \times 10^{57}$ erg for an overpressure factor of 10. Dividing the enthalpy changes by the time of release of this energy, we find the bubble luminosity. Using three estimates for the time introduced by Bîrzan et al. (2004), we evaluated the heating luminosities listed in Table 4. The sound crossing time, $t_c = \frac{R}{\sqrt{\frac{\gamma kT}{\mu m_H}}}$, is the time for the bubble to move to the current place with the sound speed in the group core. The buoyant rise time, $t_b = \frac{R}{\sqrt{\frac{2gV}{SC}}}$, is the time in which the bubble moves out buoyantly and the refill time, $t_r = 2\sqrt{\frac{r}{g}}$, is the time taken to refill the volume displaced by the bubble during the movement. Here, R is the distance between the galaxy center and the radio lobe. V and S are the volume and cross section of the bubble, respectively. C is the drag

Table 4
Energy Injection in the Core of RX J1416.4+2315

p_0/p[a]	t_r (10^7 years)	t_b (10^7 years)	t_c (10^7 years)	ΔH (10^{57} erg)	P_r (10^{42} erg s^{-1})	P_b (10^{42} erg s^{-1})	P_c (10^{42} erg s^{-1})	$L_{(x<50\ \mathrm{kpc})}$ (10^{42} erg s^{-1})	$L_{(x<130\ \mathrm{kpc})}$ (10^{43} erg s^{-1})
2	3.7	3.0	2.7	2.6	2.3	2.7	3.1	2.8	2.5
10	3.7	3.0	2.7	10.6	9.2	11.2	12.5	2.8	2.5

Note.
[a] Overpressure factor of the injected lobe.

coefficient. We assumed $C = 0.75$ (Churazov et al. 2001). g is gravitational acceleration, which is approximated by the relation $g \approx 2\sigma^2/R$, where σ is the velocity dispersion of the galaxy group ($\approx$694 km s^{-1}). r is the mean radius of the bubble, which we discussed earlier.

The X-ray study of J1416 (Khosroshahi et al. 2006a) shows that the gas within 130 kpc has a shorter cooling time than the Hubble time, while there is only a small temperature drop in the core of the galaxy group ($r < 50$ kpc) where the cooling time is $\sim$5 Gyr. The energy loss by X-ray emission is $L_x = 2.8 \times 10^{42}$ erg s^{-1} within 50 kpc and $L_x = 2.5 \times 10^{43}$ erg s^{-1} within 130 kpc. The mechanical luminosity of the radio lobe is $L_{\mathrm{mech}} = 2.2 \times 10^{42}$ erg s^{-1}, assuming an overpressure factor of 2 and $L_{\mathrm{mech}} = 1.2 \times 10^{43}$ erg s^{-1} for overpressure factors of 10 (Table 4). Thus, the estimated mechanical heating appears to be only sufficient to heat up the cool core of the group, and at higher radii other sources of heating are also required. The fact that AGN feedback can only touch the inner radius preserves self-similarity in galaxy groups and clusters. A recent study by Gaspari et al. (2014) shows that breaking the self-similar scaling relations destroys the cool core in galaxy groups and clusters and changes all systems into non-cool-core objects, which is not consistent with X-ray observations.

We note that the highest angular resolution achieved in the 610 MHz map is approximately equal to the size of the radio bubble. Since we use the radio bubble size to calculate the volume (Equation (3)), the estimated mechanical work will be the upper limit. For the Bîrzan et al. (2004) sample, the cavity dimensions vary from tens of kpc in massive clusters to a few kpc in low mass systems. Thus, our estimate for the bubble size ($\sim$12 kpc) is consistent with a typical expected size.

The properties of the core can be seen better in the hardness ratio map (Figure 8) which shows an asymmetric distribution of soft and hard regions. The bubble-like low energy cavities are marked in the map. There is no detected radio counterpart for these structures, possibly due to the synchrotron aging. Future low frequency (<610 MHz) radio observations of this object with high sensitivity will discover the nature of these cavities. All the cavities are within 130 kpc (cooling radius) from the cluster center. Assuming they emerge from multiple cycles of AGN outbursts, we estimated the mechanical power for each cavity listed in Table 3. The sound crossing time, the cluster pressure at the position of the cavity, and the overpressure factor of 10 (the maximum mechanical work) have been used to estimate the power. The total energy content of the cavities (A, C, D, and E) is $\Sigma PV = 9.6 \times 10^{58}$ erg, corresponding to the total mechanical luminosity of $L_{\mathrm{mech}} = 1.3 \times 10^{44}$ erg s^{-1}. Therefore, the heating power is completely sufficient to quench the cooling rate within 130 kpc in the cluster core. By changing the initial conditions of the inflated bubble and applying an overpressure factor of 2 (the minimum mechanical work), the heating power is hardly sufficient to stop the gas from cooling, $L_{\mathrm{mech}} = 1.9 \times 10^{43}$ erg s^{-1}. We will discuss this in Section 7.

In addition to the mechanical heating of the radio lobe, dissipation of shock waves and sound waves produced by AGN outbursts is another source of heating (McNamara & Nulsen 2007). This is illustrated by cavities, weak shocks, and filamentary structures produced by a series of AGN outbursts in the X-ray image of the M87 galaxy (Forman et al. 2007). For J1416, both *Chandra* and *XMM-Newton* in the soft band (0.5–2.0 kev) show relatively smooth emission except at the core where an X-ray extension appears in the southeast and the same direction of the radio bubble in the *XMM-Newton* map (Figure 5). It is probable that this structure is related to the AGN outburst or the result of low resolution and high smoothing of the *XMM-Newton* map. Any firm conclusions about the existence of weak shocks will require higher quality X-ray data.

Observations of a large sample of clusters and groups have helped to deduce a correlation between the radio luminosity and the jet power. Bîrzan et al. (2004) studied a sample of galaxy clusters and groups with clear X-ray cavities and derived a relation between cavity power and total radio luminosity, showing that L_{mech} is approximately proportional to $\sqrt{L_{\mathrm{radio}}}$ but the radio luminosity is on average smaller by a factor of 100.

We use the radio flux density of the central source S_{ν_0} at a frequency of $\nu_0 = 1.4$ GHz to evaluate the total radio luminosity with the assumption of a power law spectrum between $\nu_1 = 10$ MHz and $\nu_2 = 5000$ MHz and a spectral index of $\alpha = 0.83$. Using the relation

$$L_{\mathrm{radio}} = 4\pi D_L{}^2 S_{\nu_0} \int_{\nu_1}^{\nu 2} \left(\frac{\nu}{\nu_0}\right)^{-\alpha} d\nu \qquad (5)$$

we approximate the total radio luminosity to be 1.1×10^{40} erg s^{-1}. The corresponding mechanical luminosity according to the Bîrzan et al. (2004) relation is $4.1 \times 10^{42}{}^{\pm 5}$ erg s^{-1}, consistent with our results in Table 4.

5. SYNCHROTRON AGES AND THE MAGNETIC FIELD

Assuming that the radio lobe is in pressure balance with the environment, the gas pressure estimated from the X-ray observation should be equal to the lobe internal pressure. The radio lobe pressure is the sum of the particles and magnetic field pressure and is evaluated using the bolometric radio luminosity of the lobe,

$$P_{\mathrm{th}} = P_p + P_B$$

$$= \frac{(1+k)}{3V\phi} C_{12}(\alpha; \nu_1; \nu_2) B^{-3/2} L_{\mathrm{radio}} + \frac{B^2}{8\pi}. \qquad (6)$$

Here, $P_{\rm th}$ is the gas thermal pressure. k is the coefficient that relates the energy of positive particles to the energy of electrons. ϕ is the filling factor of magnetic field. C_{12} is a function of emitting first and last frequencies and the spectral index, introduced by Pacholczyk (1970). We assume the radio lobe consists of relativistic electrons and positrons ($k = 0$), with a filling factor of $\phi = 1$. The applied minimum and maximum cutoff for frequencies are $\nu_1 = 10$ MHz and $\nu_2 = 100$ GHz. Following this method, we found two solutions for the magnetic field of the lobe, $B_1 = 20\,\mu$G and $B_2 = 0.5\,\mu$G. B_2 seems to be too small according to the magnetic field strength in radio lobes (Stawartz et al. 2006). Thus, we adopted $B_1 = 20\,\mu$G, which shows that the magnetic pressure is dominated inside the radio lobe.

Unlike the radio emission at 610 MHz, there is no radio lobe in the 1420 MHz map. Assuming the same spectral index for the central source and the radio lobe, the emission of the radio lobe at 1420 MHz would be larger than 3σ of the map. Thus, there are two possibilities for explaining the lack of radio lobe detection at high frequency. First, the difference in the electron energy distribution of the lobe and the central source causes a steeper spectral index for the radio lobe. Second, the steepening emerges from synchrotron aging. The former is not likely, since both of the radio emissions originated from the central AGN while the latter is a common phenomenon observed in radio lobes. The energy of the synchrotron electrons in the plasma decreases with time because of their emission. This phenomenon defines a critical time ($t_{\rm syn}$) in which particles lose most of their energy and produces a break at the synchrotron spectrum for the frequencies beyond the critical frequencies ($\nu > \nu_c$). The break frequency (ν_c) is related to the synchrotron age via the relation

$$t_{\rm syn} = 1060 \frac{B^{1/2}}{B^2 + 2/3 {B_{\rm CMB}}^2} \left[\nu_c (1+z)\right]^{-1/2} \ {\rm Myr}. \quad (7)$$

Here, B is in μG, ν_c is in GHz, and $B_{\rm CMB} = 3.251 + z^2\,\mu$G is the equivalent cosmic microwave background (CMB) magnetic field. The electron energy also decreases due to the inverse Compton scattering of CMB photons (see Feretti & Giovannini 2008 for details). The absence of any radio lobe at 1420 MHz indicates a spectrum break below this frequency, resulting in $t_{\rm syn} \gtrsim 1 \times 10^7$ years. This is consistent with the three estimated ages for the bubble in Section 4.

6. ACCRETION AND BLACK HOLE GROWTH

In addition to the energy considerations around the heating and cooling balance at the core of galaxy groups and clusters, the energy balance of AGN feeding and feedback is required to complete the cycle of galaxy formation and growth. The SMBH accretion by hot or cold gas is widely discussed in the literature (Pizzolato & Soker 2005; McNamara et al. 2011; Gaspari et al. 2013; Yuan & Narayan 2014). The rotational energy of a rapidly spinning black hole can also power AGN activity (McNamara et al. 2009). In this section, we approximate Bondi accretion (Bondi 1952), a spherical symmetric accretion of hot gas into the central black hole, as a way to know whether or not it is sufficient to feed the central black hole. The correlation of Bondi accretion and jet power has been shown in previous studies (Allen et al. 2006; Rafferty et al. 2006).

The accretion rate is related to the temperature, density, and central black hole mass via the relation:

$$\dot{M}_{\rm bondi} = 1.66 \times 10^{-7} {M_7}^2 {T_2}^{-3/2} n_{0.1} M_{\rm Sun}\ {\rm yr}^{-1}. \quad (8)$$

We evaluate the black hole mass using the correlation between the black hole mass and the K_s luminosity (Marconi & Hunt 2003):

$$\log \frac{M_{\rm BH}}{M_{\rm Sun}} = 8.21 + 1.13 \left[\log \frac{L_K}{L_{\rm Sun}} - 10.9\right]. \quad (9)$$

The estimated black hole mass is $M_{\rm BH} = 2.4 \times 10^9 M_{\rm Sun}$. Using the core density $n_{\rm e} = 0.002\,{\rm cm}^{-3}$ and temperature $T = 4$ keV, we found an accretion rate of $\dot{M} = 6.7 \times 10^{-5}\ M_{\rm Sun}\ {\rm yr}^{-1}$, corresponding to Bondi accretion of $P_{\rm bondi} = \epsilon M c^2 = 3.8 \times 10^{41}\ {\rm erg\ s}^{-1}$. In this estimation, we assumed an efficiency factor of $\epsilon = 0.1$ for the accretion. The calculated Bondi accretion power is an order of magnitude lower than the jet power (Section 4). Note that the accretion happens within the Bondi radius. For a black hole mass $M_{\rm BH}$ and accreting gas temperature T, the Bondi radius $R_{\rm bondi}$ is:

$$R_{\rm bondi} = 0.031 \left(\frac{kT}{\rm keV}\right)^{-1} \left(\frac{M_{\rm BH}}{10^9 M_{\rm Sun}}\right) {\rm kpc}. \quad (10)$$

In the J1416 galaxy cluster, this radius is $\sim$0.02 kpc. The spatial resolution of the X-ray data does not allow us to resolve this region. Therefore, the true Bondi power must be higher than this value. Rafferty et al. (2006) discussed this correction and showed that having a bigger gap between the Bondi radius and the radius that the Bondi power has been estimated within, we observe a higher cavity–Bondi power ratio. In order to correct this effect, they assumed a power law density profile and predict the Bondi accretion rate. Applying this correction for J1416 shows that the cavity power is consistent with the Bondi power.

7. SUMMARY AND DISCUSSION

We carried out radio observations of RX J1416.4+2315, a massive fossil galaxy group, to study AGN activity and IGM heating in this object. Fossil groups are thought to be an ideal environment to study IGM heating since they show no sign of group scale mergers or major mergers of the dominant galaxy. The radio observations were performed using the GMRT radio array at 610 and 1420 MHz.

The radio emission of the central BCG is detected at both frequencies, showing a spectral index of 0.83. In 610 MHz, a radio lobe is detected in the SE of the central source. We evaluate mechanical work that is done by the radio bubble on the IGM. If the bubble blows with small overpressure ($\frac{p_0}{p} = 2$), the heating power will be $\sim 3 \times 10^{42}\ {\rm erg\ s}^{-1}$, which is sufficient to quench the cooling within a $\sim$50 kpc radius. The temperature profile of J1416 shows a slight drop in this region. If we assume that the bubble initial pressure is high ($\frac{p_0}{p} = 10$), the heat supply will be $\sim 1 \times 10^{43}\ {\rm erg\ s}^{-1}$. The total heating power that is required to completely stop cooling within the cooling radius ($\sim$130 kpc) is 2–3 $\times 10^{43}\ {\rm erg\ s}^{-1}$. Thus, the PV work is not sufficient for the entire cooling flow region. In addition to that, the X-ray hardness ratio map shows three clear cavities within the cooling radius. They might be the results of previous AGN outbursts. By taking into account all sources,

the heating power will be $\sim 10^{44}$ erg s^{-1}, which is quite sufficient to offset the cooling flow.

We estimate a Bondi accretion rate of 3.8×10^{41} erg s^{-1} for this system. The accretion power is significantly smaller than the jet power but such a difference emerges from the poor X-ray resolution. Applying the correction for the Bondi radius, we showed that Bondi accretion and jet power are consistent.

We note that there are uncertainties in estimating the mechanical heating for the various reasons.

1. The energetic content of the radio lobe is a function of the adiabatic index (Equation (3)), and depends on whether the bubble is filled with relativistic or non-relativistic plasma.
2. The large uncertainty in evaluating the heating power is clear, due to the method we used. The total enthalpy and enthalpy changes are used for this aim. Nusser et al. (2006) calculated the heating rate by introducing three phases: injected bubble, buoyant bubble, and destroyed bubble. They derived precise relations, but using the observable parameters in the deduced relations is not possible because of the low resolution of the X-ray data. Moreover, assumptions for the initial conditions, e.g., the bubble overpressure factor, change the results by an order of magnitude.
3. Uncertainty in the definition of the cooling radius based on the cooling time, temperature drop, or significant classical mass deposition rate for estimating the X-ray loss results in a huge difference in the estimated cooling power.

REFERENCES

Allen, S. W., Dunn, R. J. H., Fabian, A. C., Taylor, G. B., & Reynolds, C. S. 2006, MNRAS, 372, 21
Begelman, M. C. 2001, in ASP Conf. Ser. 240, Gas and Galaxy Evolution, ed. J. E. Hibbard, M. Rupen & J. H. van Gorkom (San Francisco, CA: ASP), 363
Bîrzan, L., McNamara, B. R., Nulsen, P. E. J., Carilli, C. L., & Wise, M. W. 2008, ApJ, 686, 859
Bîrzan, L., Rafferty, D. A., McNamara, B. R., Wise, M. W., & Nulsen, P. E. J. 2004, ApJ, 607, 800
Blanton, E. L., Clarke, T. E., Sarazin, C. L., Randall, S. W., & McNamara, B. R. 2010, PNAS, 107, 7174
Bondi, H. 1952, MNRAS, 112, 195
Cavagnolo, K. W., McNamara, B. R., Nulsen, P. E. J., et al. 2010, ApJ, 720, 1066
Churazov, E., Brüggen, M., Kaiser, C. R., Böhringer, H., & Forman, W. 2001, ApJ, 554, 261
Churazov, E., Sunyaev, R., Forman, W., & Böhringer, H. 2002, MNRAS, 332, 729
Dariush, A. A., Khosroshahi, H. G., Ponman, T. J., et al. 2007, MNRAS, 382, 433
Dariush, A. A., Raychaudhury, S., Ponman, T. J., et al. 2010, MNRAS, 405, 1873
Dunn, R. J. H., Allen, S. W., Taylor, G. B., et al. 2010, MNRAS, 404, 180
Dunn, R. J. H., & Fabian, A. C. 2004, MNRAS, 355, 862
Dunn, R. J. H., Fabian, A. C., & Taylor, G. B. 2005, MNRAS, 364, 1343
Ellison, S. L., Patton, D. R., Mendel, J. T., & Scudder, J. M. 2011, MNRAS, 418, 2043
Fabian, A. C., Nulsen, P. E. J., & Canizares, C. R. 1984, Natur, 310, 733
Fabian, A. C., Nulsen, P. E. J., & Canizares, C. R. 1991, A&ARv, 2, 191
Fabian, A. C., Sanders, J. S., Taylor, G. B., et al. 2006, MNRAS, 366, 417
Feretti, L., & Giovannini, G. 2008, in A Pan-Chromatic View of Clusters of Galaxies and the Large-Scale Structure, Vol. 740, ed. M. Plionis, O. López-Cruz & D. Hughes (Berlin: Springer), 143
Forman, W., Jones, C., Churazov, E., et al. 2007, ApJ, 665, 1057
Gaspari, M., Brighenti, F., D'Ercole, A., & Melioli, C. 2011, MNRAS, 415, 1549
Gaspari, M., Brighenti, F., Temi, P., & Ettori, S. 2014, ApJL, 783, L10
Gaspari, M., Ruszkowski, M., & Oh, S. P. 2013, MNRAS, 432, 3401
Gómez, P. L., Loken, C., Roettiger, K., & Burns, J. O. 2002, ApJ, 569, 122
Heinz, S., Brüggen, M., Young, A., & Levesque, E. 2006, MNRAS Letters, 373, 65
Hlavacek-Larrondo, J., Fabian, A. C., Edge, A. C., et al. 2012, MNRAS, 421, 1360
Hlavacek-Larrondo, J., McDonald, M., Benson, B. A., et al. 2015, ApJ, 805, 13
Jones, L. R., Ponman, T. J., Horton, A., et al. 2003, MNRAS, 343, 627
Jones, L. R., Scharf, C., Ebeling, H., et al. 1998, ApJ, 495, 100
Khosroshahi, H. G., Maughan, B., Ponman, T. J., & Jones, L. R. 2006a, MNRAS, 369, 1211
Khosroshahi, H. G., Ponman, T. J., & Jones, L. R. 2006b, MNRAS Letters, 372, 68
Khosroshahi, H. G., Ponman, T. J., & Jones, L. R. 2007, MNRAS, 377, 595
Marconi, A., & Hunt, L. K. 2003, ApJ, 589, 21
Markevitch, M., Sarazin, C. L., & Vikhlinin, A. 1999, ApJ, 521, 526
Markevitch, M., & Vikhlinin, A. 2007, PhR, 443, 1
McNamara, B. R., Kazemzadeh, F., Rafferty, D. A., et al. 2009, ApJ, 698, 594
McNamara, B. R., & Nulsen, P. E. J. 2007, ARA&A, 45, 117
McNamara, B. R., Rohanizadegan, M., & Nulsen, P. E. J. 2011, ApJ, 727, 39
Mittal, R., Hudson, D. S., Reiprich, T. H., & Clarke, T. 2009, A&A, 501, 835
Nulsen, P. E. J., Jones, C., Forman, W. R., et al. 2007, in ESO Astrophysics Symp., Heating Versus Cooling in Galaxies and Clusters of Galaxies, ed. H. Böhringer et al. (Berlin: Springer), 210
Nusser, A., Silk, J., & Babul, A. 2006, MNRAS, 373, 739
O'Sullivan, E., Giacintucci, S., David, L. P., et al. 2011, ApJ, 735, 11
Pacholczyk, A. G. 1970, Radio Astrophysics. Nonthermal Processes in Galactic and Extragalactic Sources (San Francisco, CA: Freeman)
Perlman, E. S., Horner, D. J., Jones, L. R., et al. 2002, ApJS, 140, 265
Peterson, J. R., & Fabian, A. C. 2006, PhR, 427, 1
Pizzolato, F., & Soker, N. 2005, ApJ, 632, 821
Rafferty, D. A., McNamara, B. R., Nulsen, P. E. J., & Wise, M. W. 2006, ApJ, 652, 216
Reiprich, T. H. 2001, PhD dissertation, Ludwig-Maximilians Univ. Munchen
Sanders, J. S., Fabian, A. C., & Taylor, G. B. 2009, MNRAS, 393, 71
Sarazin, C. L. 1986, RvMP, 58, 1
Scharf, C. A., Jones, L. R., Ebeling, H., et al. 1997, ApJ, 477, 79
Springel, V., Di Matteo, T., & Hernquist, L. 2005a, MNRAS, 361, 776
Springel, V., Di Matteo, T., & Hernquist, L. 2005b, ApJL, 620, 79
Stawartz, L., Kneiske, T. M., & Kataoka, J. 2006, ApJ, 637, 693
Yuan, F., & Narayan, R. 2014, ARA&A, 52, 529